

Absolute versus convective helical magnetorotational instability in a Taylor-Couette flow

Jānis Priede*

Applied Mathematics Research Centre, Coventry University, Coventry, CV1 5FB, United Kingdom

Gunter Gerbeth

Department of MHD, Forschungszentrum Dresden-Rossendorf, P.O. Box 510119, D-01314 Dresden, Germany

We analyze numerically the magnetorotational instability of a Taylor-Couette flow in a helical magnetic field [helical magnetorotational instability (HMRI)] using the inductionless approximation defined by a zero magnetic Prandtl number ($Pm = 0$). The Chebyshev collocation method is used to calculate the eigenvalue spectrum for small amplitude perturbations. First, we carry out a detailed conventional linear stability analysis with respect to perturbations in the form of Fourier modes that corresponds to the convective instability which is not in general self-sustained. The helical magnetic field is found to extend the instability to a relatively narrow range beyond its purely hydrodynamic limit defined by the Rayleigh line. There is not only a lower critical threshold at which HMRI appears but also an upper one at which it disappears again. The latter distinguishes the HMRI from a magnetically modified Taylor vortex flow. Second, we find an absolute instability threshold as well. In the hydrodynamically unstable regime before the Rayleigh line, the threshold of absolute instability is just slightly above the convective one although the critical wavelength of the former is noticeably shorter than that of the latter. Beyond the Rayleigh line the lower threshold of absolute instability rises significantly above the corresponding convective one while the upper one descends significantly below its convective counterpart. As a result, the extension of the absolute HMRI beyond the Rayleigh line is considerably shorter than that of the convective instability. The absolute HMRI is supposed to be self-sustained and, thus, experimentally observable without any external excitation in a system of sufficiently large axial extension.

PACS numbers: 47.20.Qr, 47.65.-d, 95.30.Lz

I. INTRODUCTION

The magnetorotational instability (MRI) is known to be able to destabilize hydrodynamically stable flows by means of an externally imposed magnetic field as originally shown by Velikhov [1] and analyzed in more detail by Chandrasekhar [2] for cylindrical Taylor-Couette flow of a perfectly conducting fluid subject to an axial magnetic field. Three decades later Balbus and Hawley [3] suggested that, in a similar way, the hydrodynamically stable Keplerian velocity distribution in accretion disks could be rendered turbulent by the MRI accounting for the formation of stars and entire galaxies proceeding much faster than it could be accomplished by the viscous angular-momentum transport alone. Meanwhile this proposition has triggered not only numerous theoretical and numerical studies [4] but also some experimental efforts as well [5, 6]. However, one of the main technical challenges to laboratory MRI is the magnetic Reynolds number Rm which is required to be ~ 10 at least. For a liquid metal with the magnetic Prandtl number $Pm \sim 10^{-5} - 10^{-6}$ this translates into a hydrodynamic Reynolds number $Re = Rm/Pm \sim 10^6 - 10^7$ [7]. Thus, the base flow on which the MRI is supposed to be observable may easily be turbulent at such Reynolds

numbers independently of MRI as in the experiment of Sisan *et al.* [5]. A way to circumvent this problem was proposed by Hollerbach and Rüdiger [8] who suggested that MRI can take place in the Taylor-Couette flow at $Re \sim 10^3$ when the imposed magnetic field is helical rather than purely axial as in the classical case. The theoretical prediction of this new type of helical MRI (HMRI) was soon succeeded by a confirming experimental evidence provided by the so-called PROMISE facility [9, 10, 11]. Nevertheless, these experimental observations have subsequently been questioned by Liu *et al.* [12] who find no such instability in their inviscid theoretical analysis of finite length cylinders with insulating end caps. They suspect the observed phenomenon to be a transient growth rather than a self-sustained instability [13, 14].

Indeed, such an interpretation of the HMRI is possible when the analysis is based only on the conventional linear stability analysis for separate Fourier modes as done by Hollerbach and Rüdiger [8] following the classical MRI approach. However, there is a principal difference between the classical and the helical MRIs, namely, the former is stationary whereas the latter is traveling. It is important to emphasize that the conventional stability analysis for traveling waves yields the so-called convective instability threshold at which the system becomes able to amplify certain externally excited perturbations. At this threshold the perturbation grows in time only in the frame of reference moving with its group velocity while it asymptotically decays in any other frame of

*Electronic address: J.Priede@coventry.ac.uk

reference including the laboratory one [15]. Eventually, such a growing while traveling perturbation reaches the end wall where it is absorbed unless the system is able to reflect it back. The latter supposes reflection symmetry in the system which, however, is not the case provided that the magnetic field is helical. Thus, it is indeed unclear whether the HMRI can be self-sustained in an ideal Taylor-Couette flow of large but finite axial extension.

This question is addressed in the second part of the present study where the absolute HMRI is found to exist besides the convective one which, in turn, is analyzed in detail in the first part. Note that the existence of absolute instability is nontrivial as known, for instance, for the Ponomarenko dynamo [16] which has a convective but no absolute instability threshold [17]. The latter requires an additional return flow to be included in the original Ponomarenko model [18]. The distinction between convective and absolute instabilities is relevant mainly for open flows and unbounded geometries [19]. In finite geometries, it is important to distinguish transiently growing and noise-sustained perturbations from the self-sustained linear instabilities, which are always global with the threshold asymptotically approaching from above that of the absolute instability as the system size increases [20, 21].

We consider both the convective and the absolute HMRI in the inductionless approximation corresponding to $\text{Pm} = 0$ that was suggested in our previous work [22]. This approximation, which leads to a significant simplification of the problem, allows us to focus exclusively on the HMRI because it does not capture the conventional MRI [23]. We show that the HMRI is effective only in a relatively narrow range of the ratio of rotation rates of the inner and outer cylinders beyond the limit of purely hydrodynamic instability defined by the so-called Rayleigh line. For the convective HMRI, the range of instability is considerably larger for perfectly conducting cylinders than that for insulating ones. In addition we find that the HMRI is effective only in a limited range of Reynolds numbers. Namely, for any unstable mode, there is not only a lower critical Reynolds number by exceeding which the HMRI sets in but also an upper one by exceeding which it disappears again. It is this upper threshold that distinguishes HMRI from a magnetically modified Taylor vortex flow. Absolute HMRI exists in a significantly narrower range of parameters than the convective one. In contrast to the convective HMRI, the absolute one is much less dependent on the conductivity of the boundaries.

The paper is organized as follows. In Sec. II we formulate the problem using the inductionless approximation. Numerical results concerning the convective and absolute instability thresholds for both insulating and perfectly conducting cylinders are presented in Secs. III A and III B, respectively. Section IV concludes the paper with a summary and a comparison with experimental results of Stefani *et al.* [9, 10, 11].

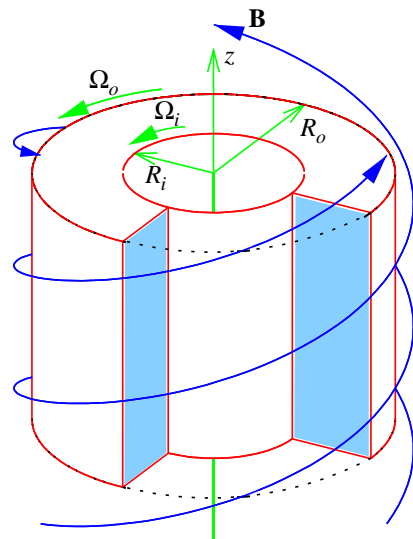


Figure 1: Sketch to the formulation of the problem.

II. PROBLEM FORMULATION

Consider an incompressible fluid of kinematic viscosity ν and electrical conductivity σ filling the gap between two infinite concentric cylinders with inner radius R_i and outer radius R_o rotating with angular velocities Ω_i and Ω_o , respectively, in the presence of an externally imposed steady magnetic field $\mathbf{B}_0 = B_\phi \mathbf{e}_\phi + B_z \mathbf{e}_z$ with axial and azimuthal components $B_z = B_0$ and $B_\phi = \beta B_0 R_i / r$ in cylindrical coordinates (r, ϕ, z) , where β is a dimensionless parameter characterizing the geometrical helicity of the field (Fig. 1). Further, we assume the magnetic field of the currents induced by the fluid flow to be negligible relative to the imposed field. This corresponds to the so-called inductionless approximation holding for most of liquid-metal magnetohydrodynamics characterized by small magnetic Reynolds numbers $\text{Rm} = \mu_0 \sigma v_0 L \ll 1$, where μ_0 is the magnetic permeability of vacuum and v_0 and L are the characteristic velocity and length scale. The velocity of fluid flow \mathbf{v} is governed by the Navier-Stokes equation with electromagnetic body force

$$\frac{\partial \mathbf{v}}{\partial t} + (\mathbf{v} \cdot \nabla) \mathbf{v} = -\frac{1}{\rho} \nabla p + \nu \nabla^2 \mathbf{v} + \frac{1}{\rho} \mathbf{j} \times \mathbf{B}_0, \quad (1)$$

where the induced current follows from Ohm's law for a moving medium

$$\mathbf{j} = \sigma (\mathbf{E} + \mathbf{v} \times \mathbf{B}_0). \quad (2)$$

In addition, we assume the characteristic time of velocity variation to be much longer than the magnetic diffusion time $\tau_0 \gg \tau_m = \mu_0 \sigma L^2$ that leads to the quasi-stationary approximation, according to which $\nabla \times \mathbf{E} = 0$ and $\mathbf{E} = -\nabla \Phi$, where Φ is the electrostatic potential. Mass and charge conservations imply $\nabla \cdot \mathbf{v} = \nabla \cdot \mathbf{j} = 0$.

The problem admits a base state with a purely az-

imathal velocity distribution $\mathbf{v}_0(r) = \mathbf{e}_\phi v_0(r)$, where

$$v_0(r) = r \frac{\Omega_o R_o^2 - \Omega_i R_i^2}{R_o^2 - R_i^2} + \frac{1}{r} \frac{\Omega_o - \Omega_i}{R_o^{-2} - R_i^{-2}}.$$

Note that the magnetic field does not affect the base flow because it gives rise only to the electrostatic potential $\Phi_0(r) = B_0 \int v_0(r) dr$ whose gradient compensates the induced electric field, so that there is no current in the base state ($\mathbf{j}_0 = 0$). However, a current may appear in a perturbed state,

$$\left\{ \begin{array}{l} \mathbf{v}, p \\ \mathbf{j}, \Phi \end{array} \right\}(\mathbf{r}, t) = \left\{ \begin{array}{l} \mathbf{v}_0, p_0 \\ \mathbf{j}_0, \Phi_0 \end{array} \right\}(r) + \left\{ \begin{array}{l} \mathbf{v}_1, p_1 \\ \mathbf{j}_1, \Phi_1 \end{array} \right\}(\mathbf{r}, t)$$

where \mathbf{v}_1 , p_1 , \mathbf{j}_1 , and Φ_1 present small-amplitude perturbations for which Eqs. (1) and (2) after linearization take the form

$$\frac{\partial \mathbf{v}_1}{\partial t} + (\mathbf{v}_1 \cdot \nabla) \mathbf{v}_0 + (\mathbf{v}_0 \cdot \nabla) \mathbf{v}_1 = -\frac{1}{\rho} \nabla p_1 + \nu \nabla^2 \mathbf{v}_1 + \frac{1}{\rho} \mathbf{j}_1 \times \mathbf{B}_0, \quad (3)$$

$$\mathbf{j}_1 = \sigma (-\nabla \Phi_1 + \mathbf{v}_1 \times \mathbf{B}_0). \quad (4)$$

In the following, we focus on axisymmetric perturbations which are typically much more unstable than nonaxisymmetric ones [24]. For such perturbations the solenoidity constraints are satisfied by meridional stream functions for fluid flow and electric current as

$$\mathbf{v} = v \mathbf{e}_\phi + \nabla \times (\psi \mathbf{e}_\phi), \quad \mathbf{j} = j \mathbf{e}_\phi + \nabla \times (h \mathbf{e}_\phi).$$

Note that h is the azimuthal component of the induced magnetic field which is used subsequently instead of Φ for the description of the induced current. Thus, we effectively retain the azimuthal component of the induction equation to describe meridional components of the induced current while the azimuthal current is explicitly related to the radial velocity. The use of the electrostatic potential Φ , which provides an alternative mathematical formulation for the induced currents in the inductionless approximation, would result in slightly more complicated governing equations. In addition, for numerical purposes, we introduce also the vorticity $\boldsymbol{\omega} = \boldsymbol{\omega} \mathbf{e}_\phi + \nabla \times (v \mathbf{e}_\phi) = \nabla \times \mathbf{v}$ as an auxiliary variable. The perturbation is sought in the normal mode form

$$\{v_1, \omega_1, \psi_1, h_1\}(\mathbf{r}, t) = \left\{ \hat{v}, \hat{\omega}, \hat{\psi}, \hat{h} \right\}(r) e^{\gamma t + ikz}, \quad (5)$$

where γ is, in general, a complex growth rate and k is the axial wave number which is real for the conventional stability analysis and complex for absolute instability. Henceforth, we proceed to dimensionless variables by using R_i , R_i^2/ν , $R_i \Omega_i$, B_0 , and $\sigma B_0 R_i \Omega_i$ as the length, time, velocity, magnetic field, and current scales, respectively. The nondimensionalized governing equations then read as

$$\gamma \hat{v} = D_k \hat{v} + \text{Re} ik (r^2 \Omega)' r^{-1} \hat{\psi} + \text{Ha}^2 ik \hat{h}, \quad (6)$$

$$\gamma \hat{\omega} = D_k \hat{\omega} + 2 \text{Re} ik \Omega \hat{v} - \text{Ha}^2 ik (ik \hat{\psi} + 2\beta r^{-2} \hat{h}), \quad (7)$$

$$0 = D_k \hat{\psi} + \hat{\omega}, \quad (8)$$

$$0 = D_k \hat{h} + ik(\hat{v} - 2\beta r^{-2} \hat{\psi}), \quad (9)$$

where $D_k f \equiv r^{-1} (r f')' - (r^{-2} + k^2) f$ and the prime stands for d/dr , $\text{Re} = R_i^2 \Omega_i / \nu$ and $\text{Ha} = R_i B_0 \sqrt{\sigma / (\rho \nu)}$ are Reynolds and Hartmann numbers, respectively, and

$$\Omega(r) = \frac{\lambda^{-2} - \mu + r^{-2} (\mu - 1)}{\lambda^{-2} - 1}$$

is the dimensionless angular velocity of the base flow defined by $\lambda = R_o/R_i$ and $\mu = \Omega_o/\Omega_i$. The boundary conditions for the flow perturbation on the inner and outer cylinders at $r = 1$ and $r = \lambda$, respectively, are $\hat{v} = \hat{\psi} = \hat{\psi}' = 0$. Boundary conditions for \hat{h} on insulating and perfectly conducting cylinders, respectively, are $\hat{h} = 0$ and $(r \hat{h})' = 0$ at $r = 1; \lambda$.

The governing equations (6)–(9) for perturbation amplitudes were discretized using a spectral collocation method on a Chebyshev-Lobatto grid with a typical number of internal points $N = 32 - 96$. Auxiliary Dirichlet boundary conditions for $\hat{\omega}$ were introduced and then numerically eliminated to satisfy the no-slip boundary conditions $\hat{\psi}' = 0$. The electric stream function \hat{h} was expressed in terms of \hat{v} and $\hat{\psi}$ by solving Eq. (9) and then substituted in Eqs. (6) and (7) that eventually resulted in the $2N \times 2N$ complex matrix eigenvalue problem which was solved by the LAPACK's ZGEEV routine.

III. NUMERICAL RESULTS

A. Convective instability

In this section, we consider the so-called convective instability threshold supplied by the conventional linear stability analysis with real wave numbers k , as done in most of previous studies [8, 10, 22]. Note that at the convective instability threshold the system becomes able to amplify certain perturbations which however might be not self-sustained and, thus, experimentally unobservable without an external excitation. The following results concern the radii ratio of outer to inner cylinder $\lambda = 2$ and we start with insulating cylinders which form the side walls of the system.

1. Insulating cylinders

The critical Reynolds number, wave number, and frequency are shown in Fig. 2 versus the angular velocity ratio μ of outer to inner cylinder for Hartmann number $\text{Ha} = 15$ and various geometrical helicities β . For $\beta = 0$ corresponding to a purely axial magnetic field, the critical Reynolds number tends to infinity as μ approaches the Rayleigh line $\mu_c = \lambda^{-2} = 0.25$ defined by $d(r^2 \Omega)/dr = 0$. Thus, for $\beta = 0$, the range of instability is limited by the Rayleigh line, *i.e.*, $\mu < \mu_c$, as in the purely hydrodynamic case. For helical magnetic fields defined by $\beta \neq 0$, the instability extends well beyond the Rayleigh line, as originally found by Hollerbach

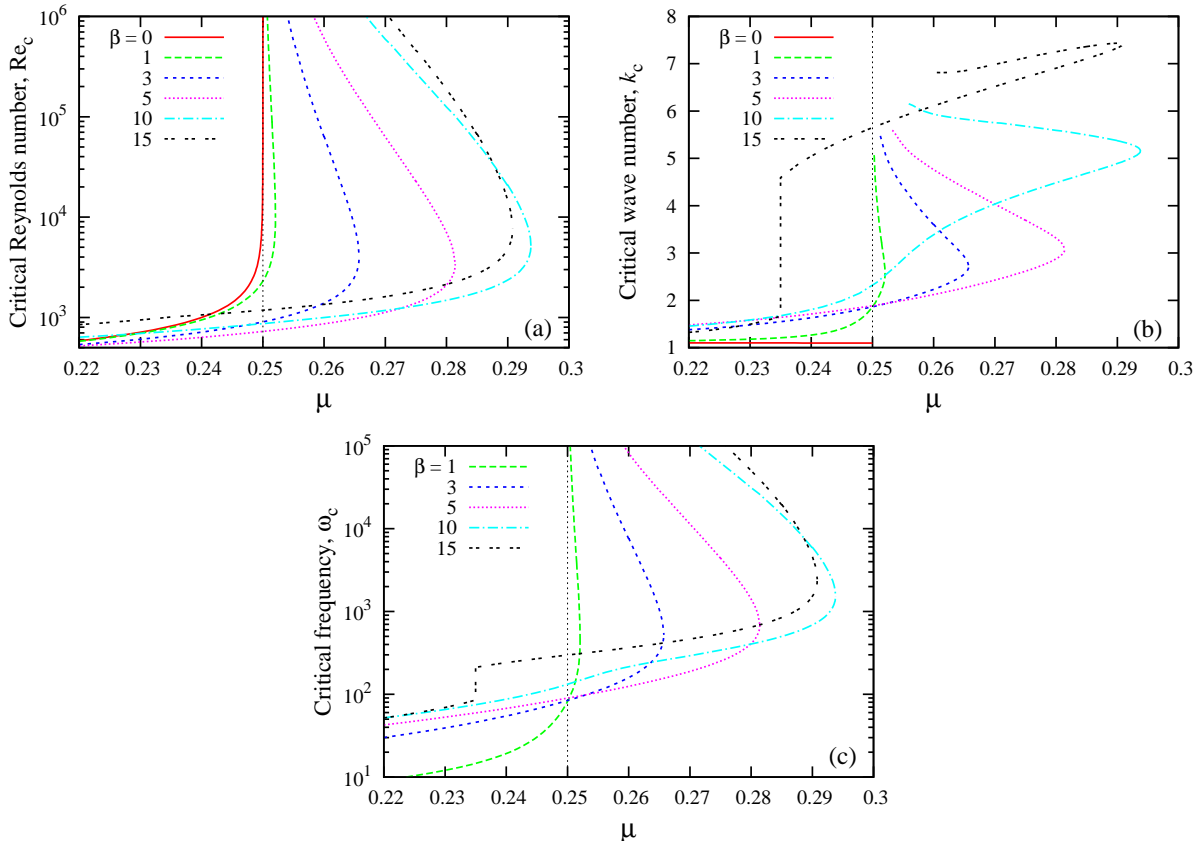


Figure 2: (a) Critical Reynolds number Re_c , (b) wave number k_c , and (c) frequency ω_c versus μ at Hartmann number $Ha = 15$ and various helicities of the magnetic field for insulating cylinders.

and Rüdiger [8]. Note that it is this extension of the instability beyond its purely hydrodynamic limit, that for ideal Taylor-Couette flow is defined by the Rayleigh line, which constitutes the essence of the MRI. Comparing the stability curves presented in Fig. 2(a) for fixed Ha to those of Hollerbach and Rüdiger [8], which are presented for $Pm \neq 0$ and variable Ha yielding minimal Re_c , there are two differences to note. First, the range of instability is limited by a certain μ_{max} , which depends on the helicity β and the Hartmann number, as shown in Fig. 13(a). Second, the destabilization beyond the Rayleigh line is effective only in a limited range of Reynolds numbers bounded by an upper critical value which tends to infinity as μ approaches the Rayleigh line from the right.

The origin of the upper critical Reynolds number, by exceeding which the flow becomes linearly stable again, is illustrated in Fig. 3 showing (a) the Reynolds number and (b) the corresponding frequency of marginally stable modes versus their wave number k for $\beta = 5$, $Ha = 15$, and $\mu = 0.27$. As seen, the marginal stability curves for μ beyond the Rayleigh line ($\mu > 0.25$) form closed loops which collapse at $\mu = \mu_{max}$. Thus, unstable modes exist only within limited ranges of wave and Reynolds numbers. Obviously, at sufficiently large Reynolds numbers the flow becomes effectively non-magnetic as inertia

starts to dominate over the electromagnetic forces suppressing the HMRI.

Note that the suppression of HMRI at high Re is related to the negligibility of the induced magnetic field as long as $Rm \ll 1$. In this case, the electric current is induced only by the velocity perturbation crossing the imposed magnetic field. In the conventional MRI conversely to the HMRI, also the induced field is relevant, which crossed by the base flow induces an additional electric current. These two effects are easily noticeable in the induction equation. Thus, in the HMRI, the resulting electromagnetic force is not affected by the base flow which is not the case for the conventional MRI, where the electromagnetic force remains significant with respect to inertia also at high Re .

As seen in Figs. 4(a) and 4(b), the critical Reynolds number can vary with the Hartmann number in three different ways depending on μ . For $\mu = 0$, the critical Reynolds number is bounded at $Ha = 0$ because a purely hydrodynamic instability is possible before the Rayleigh line. Numerical results evidence that the increase in the Hartmann number results in the growth of the critical Reynolds number with asymptotics $\sim Ha$. For $\mu = 0.25$, which lies exactly on the Rayleigh line, the flow is hydrodynamically stable without the magnetic field. Thus,

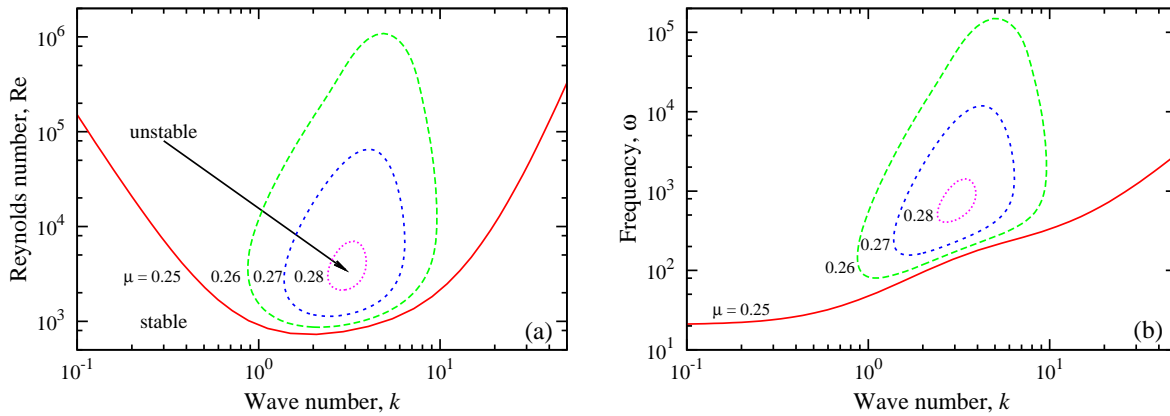


Figure 3: Neutral stability curves: (a) marginal Reynolds number and (b) the frequency versus the wave number for $\beta = 5$ and $Ha = 15$ at various ratios μ of angular velocities of the outer to inner cylinder.

in this case, the critical Reynolds number increases as $\sim Ha^{-2}$ as $Ha \rightarrow 0$ because there is no finite value of the critical Reynolds number without the magnetic field. The corresponding critical wave number tends to a finite value independent of β . With increase in the Hartmann number, the critical Reynolds number attains a minimum at $Ha \sim 10$ and starts to grow at larger Hartmann numbers similarly to the previous case. The corresponding critical wave number decreases asymptotically as $\sim Ha^{-1}$ that means a critical wavelength increasing directly with the magnetic field strength. The critical frequency plotted in Fig. 4 changes from a constant value of 30 at small Ha to another nearly constant value of about 100 slightly varying with β at large Ha . At large helicities ($\beta = 15$), another relatively short-wave instability mode dominates up to a Hartmann number $Ha \approx 30$, where the most unstable mode switches back to the long-wave one which is characteristic for smaller helicities. Transition to this large- β mode is also obvious in Fig. 2 for $\beta = 15$ at $\mu \approx 0.235$. As seen in Fig. 4(b) for $\mu = 0.27$, which is beyond the Rayleigh line, there is no instability as $Ha \rightarrow 0$. Consequently, a finite minimal value of Ha depending on β is necessary in this case. Moreover, the instability is limited by the upper branch of the critical Reynolds number discussed above which merges with the lower branch at the minimum of the Hartmann number for the given helicity β .

The variation of the critical Reynolds number with the helicity β shown in Fig. 5(a) for $\mu = 0.25 = \mu_c$ lying exactly on the Rayleigh line differs considerably from the other case with $\mu = 0.27 > \mu_c$ [see Fig. 5b]. In the first case, the flow can be destabilized by the magnetic field of however small helicity $\beta \rightarrow 0$ that results in the critical Reynolds number increasing as $\sim 1/\beta$. For $\mu > \mu_c$, a certain minimal helicity depending on the Hartmann number is needed. Moreover, in this case, there is also an upper critical Reynolds number. In both cases, there is some optimal $\beta \approx 5 - 8$ at which the lower critical Reynolds attains a minimum. Further increase in β re-

sults in the growth of the critical Reynolds number with a significantly different asymptotic behavior in both considered cases. For $\mu > \mu_c$, there is a maximal β depending on the Hartmann number at which the upper and lower branches of the critical Reynolds number merge together and the instability disappears whereas there seems to be no such merging point at any finite β when $\mu = \mu_c$. The critical wave number plotted in Figs. 5(c) and 5(d) is seen to increase with β with some jumps at larger Ha as discussed above.

2. Perfectly conducting cylinders

For perfectly conducting cylinders, the marginal stability curves shown in Fig. 6 differ considerably from those for insulating walls (see Fig. 3). Although in both cases beyond the Rayleigh line large wave numbers ($k \gg 1$) are always stable, the range of instability for perfectly conducting cylinders at moderate $\beta \lesssim 10$ extends to arbitrary small wave numbers $k \rightarrow 0$ whereas for insulating cylinders it is limited to sufficiently large k . As in the insulating case, for each unstable mode there is not only the lower but also the upper marginal Reynolds number both increasing as $\sim 1/k$ toward small k . Thus, the increase in the Reynolds number results in the shift of instability to smaller wave numbers, *i.e.*, longer waves. As a result, there is no upper critical Reynolds number for moderate $\beta \lesssim 10$ when both cylinders are perfectly conducting.

Consequently, as seen in Figs. 7(a) and 7(b), the critical Reynolds number becomes very large while the critical wave number tends to zero as μ approaches some critical μ_{\max} which varies with β . The critical frequency ω_c shown in Fig. 7(c) tends, respectively, to some finite value. This behavior changes at larger β becoming similar to that for insulating cylinders. As seen in Fig. 7(a), for $\beta \gtrsim 10$, the curves of the critical Reynolds number start to bend back at μ_{\max} toward smaller μ rather than tend to infinity. The corresponding critical wave

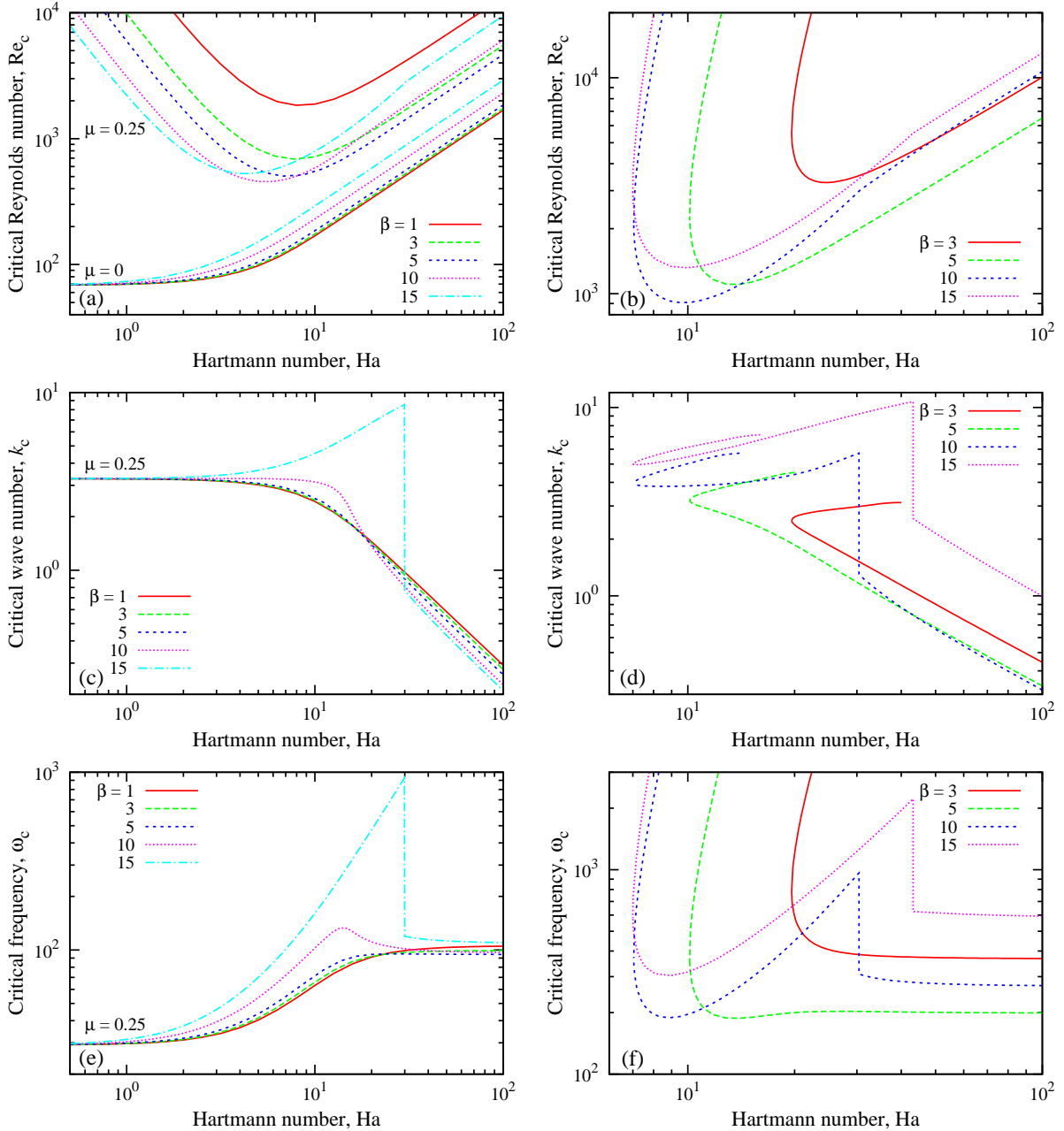


Figure 4: [(a) and (b)] Critical Reynolds number Re_c , [(c) and (d)] wave number k_c , and [(e) and (f)] frequency ω_c versus the Hartmann number for (a) $\mu = 0$, [(a), (c), and (e)] 0.25, and [(b), (d), and (f)] 0.27 at various helicities β and insulating cylinders.

numbers remain finite whereas the critical frequency increases with the Reynolds number [see Figs. 7b and 7c]. At intermediate β the limiting value of μ_{\max} , up to which the instability extends beyond the Rayleigh line, is seen in Fig. 13(a) to attain a maximum which is considerably larger than that for insulating walls. At larger β , the limiting values μ_{\max} decrease approaching those for insulating walls.

The dependence of the critical Reynolds number on the Hartmann number plotted in Fig. 8(a) at various helici-

ties is similar to that for insulating cylinders. First, Re_c attains a minimum at $Ha = 7 - 10$ and a finite minimal value of the Hartmann number is required for instability when $\mu > \mu_c$. For moderate $\beta \lesssim 10$, in contrast to the insulating case, Re_c and k_c tend to infinity and zero, respectively, as the Hartmann number approaches this minimal value which depends on β . For $\beta \gtrsim 10$, the critical Re_c has an upper branch which merges with the lower one at the minimal value of Ha as in the case of insulating cylinders. At sufficiently large Hartmann numbers,

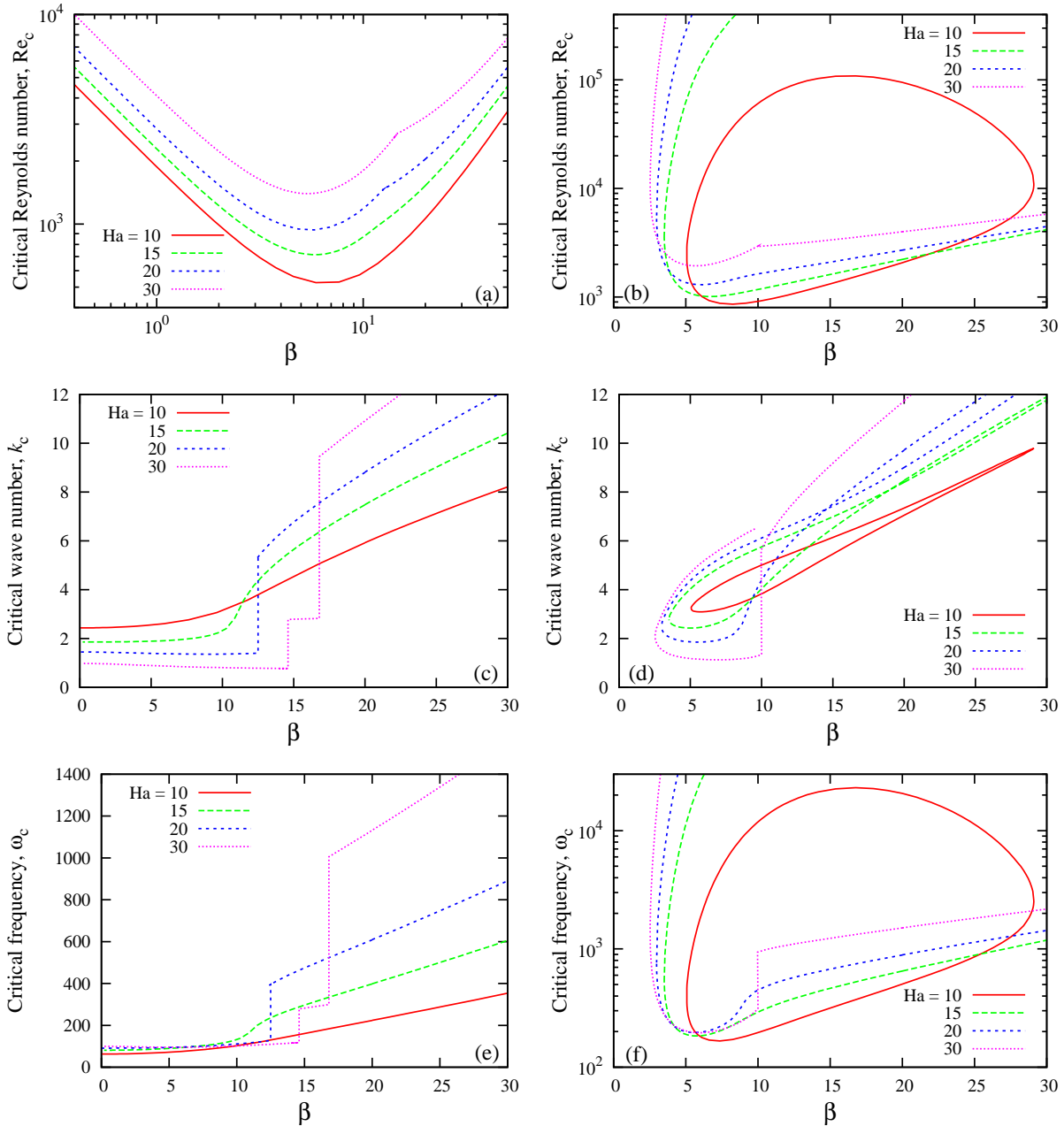


Figure 5: [(a) and (b)] Critical Reynolds number Re_c , [(c) and (d)] wave number k_c , and [(e) and (f)] frequency ω_c versus β for [(a), (c), and (e)] $\mu = 0.25$ and [(b), (d), and (f)] $\mu = 0.27$ at various Hartmann numbers.

the instability is seen to switch to a long-wave mode with the critical wave numbers and Reynolds numbers varying asymptotically as $\sim Ha^{-1}$ and $\sim Ha$, respectively.

B. Absolute instability

In this section, we turn to the absolute instability for which the wave number k is in general a complex quantity with real and imaginary parts k_r and k_i , respectively [26, 29]. It is important to realize that the convective in-

stability threshold considered above is not sufficient for the development of a self-sustained instability unless the system is mirror symmetric along the direction of propagation which, however, is not the case when the magnetic field is helical. The convective instability just ensures the ability of the system to amplify external perturbations excited with the critical frequency. From the mathematical point of view, the problem is that in an axially bounded system the perturbation has to meet certain boundary conditions at two end walls that, however, can not be accomplished by a single Fourier mode. When

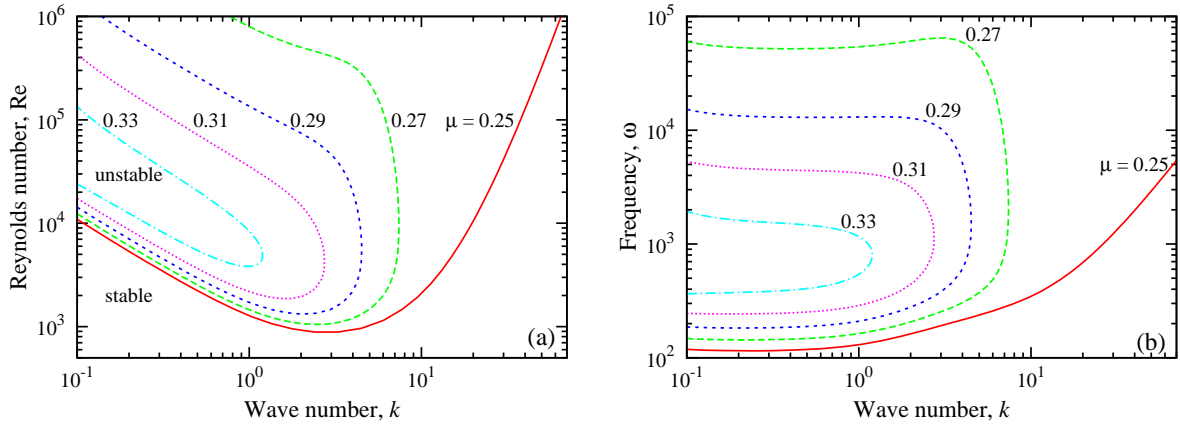


Figure 6: Neutral stability curves: (a) marginal Reynolds number and (b) the frequency versus the wave number for $\beta = 5$ and $Ha = 15$ at various ratios μ of angular velocities of the outer to inner cylinder.

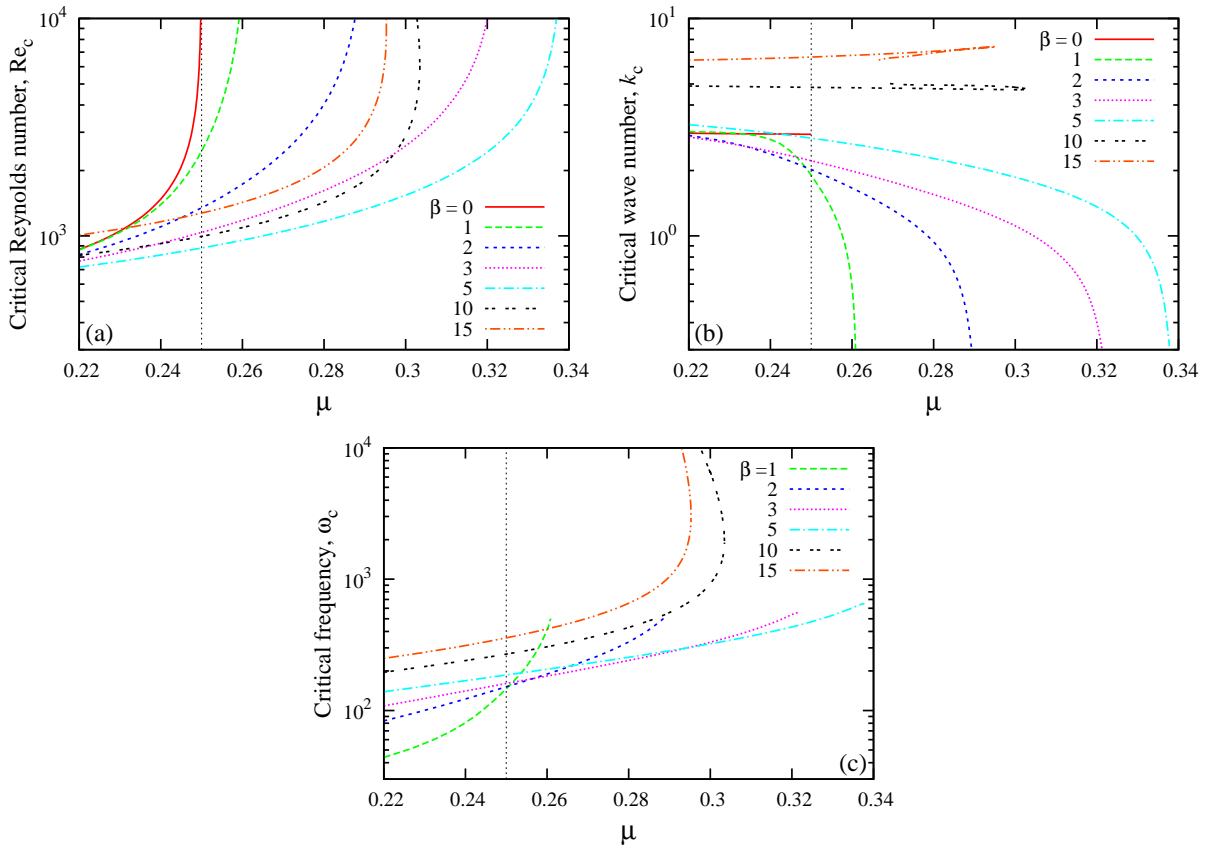


Figure 7: (a) Critical Reynolds number Re_c , (b) wave number k_c , and (c) frequency ω_c versus μ for Hartmann numbers $Ha = 15$ and various magnetic field helicities (perfectly conducting cylinders).

the critical Fourier mode is replaced with a corresponding wave packet of a limited spatial extension, one finds such a perturbation to grow only in the frame of reference traveling with its group velocity while it decays asymptotically in any other frame of reference including the laboratory one which is at rest. The growth of a perturbation in the laboratory frame of reference is en-

sured by the absolute instability threshold, at which the group velocity of the wave packet becomes zero. Thus, formally, the absolute instability requires one more condition to be satisfied, *i.e.*, zero group velocity, by means of an additional free parameter—the imaginary part of the wave number. Note that although the group velocity in non-conservative media is, in general, a complex

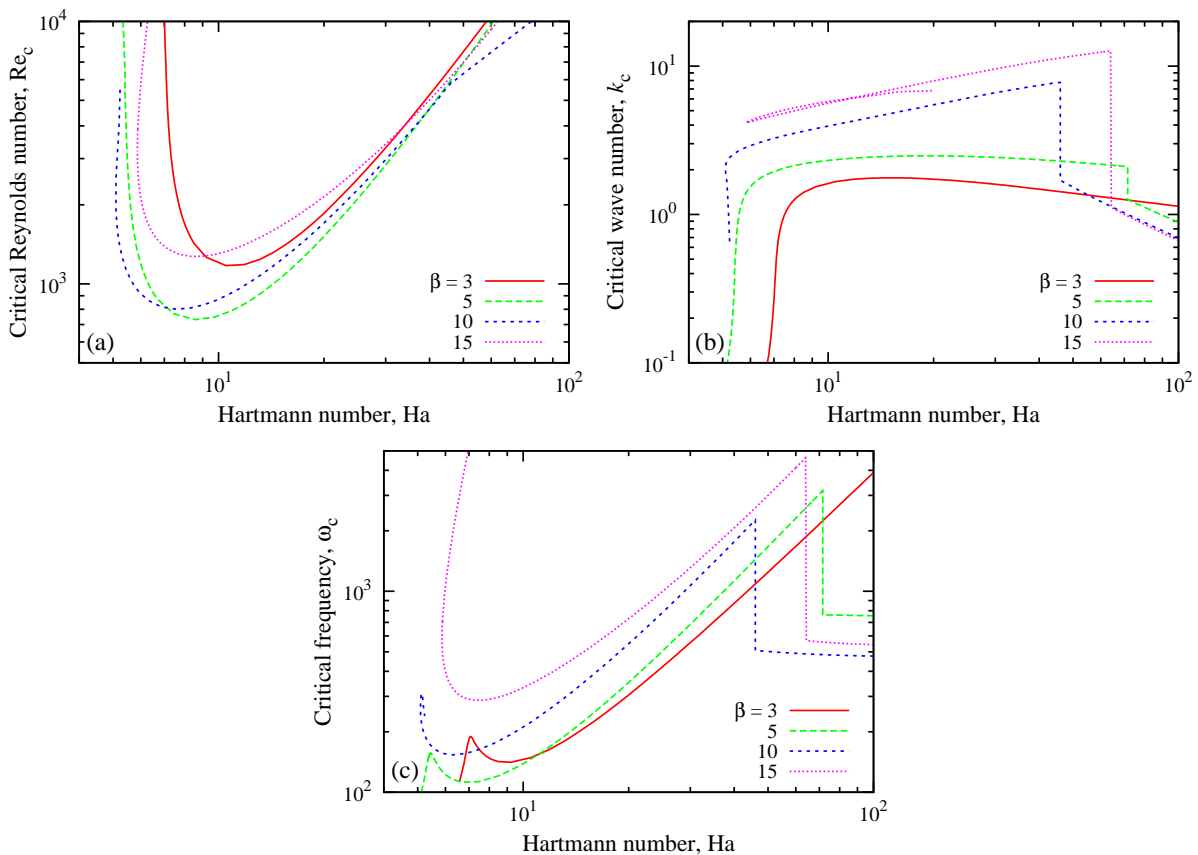


Figure 8: (a) Critical Reynolds number Re_c , (b) wave number k_c , and (c) frequency ω_c versus the Hartmann number for $\mu = 0.27$ at various helicities β and perfectly conducting cylinders.

quantity, for the most dangerous perturbations satisfying $\partial\gamma_r/\partial k_r = 0$, it is real and, thus, coincides with its common definition.

Alternatively, the absolute instability may be regarded as an asymptotic case of the global instability when the axial extension of the system becomes very large [15, 25, 26]. The basic idea is that for a convectively unstable perturbation to become self-sustained a feedback mechanism is needed which could transfer a part of the growing perturbation as it leaves the system back to its origin. Such a feedback can be provided by the reflections of perturbation from the end walls or, generally, by the end regions where the base state becomes axially non-uniform. If the base state is both stationary and axially uniform, the coefficients of the linearized perturbation equations do not depend on time and on the axial coordinate, respectively. Then, as for linear differential equations with constant coefficients, the particular solution for the perturbation varies exponentially in both time and axial coordinate as supposed by Eq. (5) where both the growth rate γ and the wave number k may be in general complex. At the end walls, where the base state is no longer axially invariant, the particular solutions with different wave numbers become linearly coupled while their time variation remains unaffected as

long as the base state is stationary. Thus, the reflection of a perturbation by the end wall in general couples modes with different wave numbers but with the same γ . Sufficiently far away from the end walls the reflected perturbation is dominated by the mode with the imaginary part of the wave number k_i corresponding to either the largest growth or lowest decay rate along the axis. Consequently, sufficiently away from the end walls a global mode is expected to consist of two such waves coupled by reflections from the opposite end walls. Taking into account that the amplitude of the reflected wave is proportional to that of the incident wave, it is easy to find that in a sufficiently extended system both waves must have the same imaginary part k_i of the wave number whereas the real parts may be different. Additionally, for two such waves to be coupled by reflections from the end walls, they have to propagate in opposite directions.

1. Insulating cylinders

We search for such a pair of modes by considering the conventional neutral stability curves at various k_i . As seen in Figs. 9(a) and (b), the increase in k_i , on one hand, results in the reduction in the wave number range

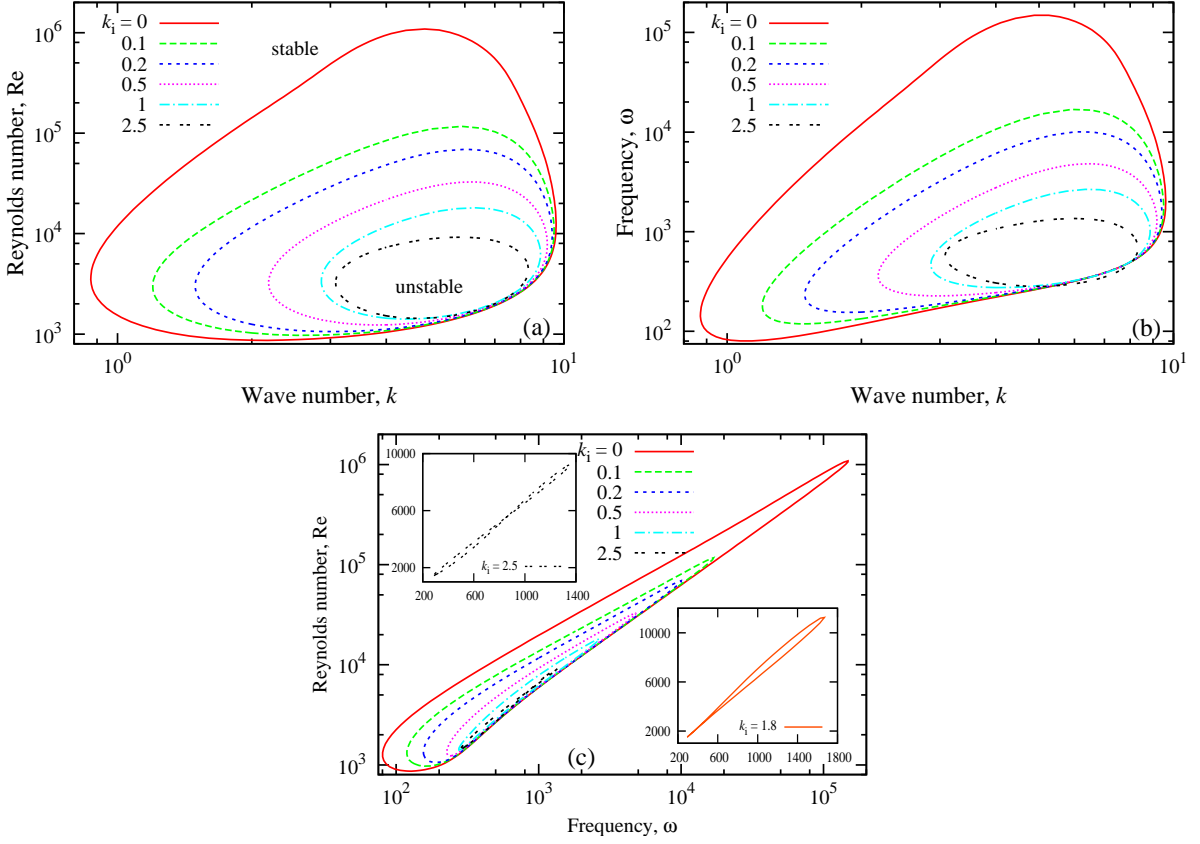


Figure 9: Neutral stability curves: (a) marginal Reynolds number and (b) the frequency versus the wave number, and (c) the Reynolds number versus the frequency for $\mu = 0.26$, $\beta = 5$, and $Ha = 15$ at various imaginary parts of wave number k_i .

admitting such neutrally stable modes. On the other hand, the lower branch of marginal Re and the corresponding frequency first increase with k_i in the whole wave number range and then start to decrease at larger k_r when k_i becomes sufficiently large ($k_i \gtrsim 1.8$). However, more important information is obtained by plotting the marginal Re and frequency from the previous curves against each other as in Fig. 9(c). First, similarly to the previous curves, these ones also form closed loops that shrink as k_i is increased. It is important to notice that at sufficiently large k_i these loops start to intersect themselves in some point as shown in the inset at the top of Fig. 9(c). This self-intersection, which is of primary importance here, occurs only in the limited range of positive k_i . The point of intersection means that at the given Reynolds number there are two modes with the same frequency and the same imaginary but possibly different real parts of the wave number. As discussed above, two such modes could be coupled by reflections from the end walls and thus form a neutrally stable global mode in an axially bounded system provided that they propagate in opposite directions [25, 26]. To determine the direction of propagation we use a local criterion [27] which we showed to be equivalent to the Briggs pinching criterion [28] for the upper instability branch at the given k_i .

Namely, the direction of propagation of both intersecting branches can be deduced from their variation with k_i . If upon a small variation of k_i one branch rises to higher Re while the other descends to lower Re , which is the case here, it can be shown that both intersecting branches correspond to oppositely propagating modes. The lowest possible Reynolds number admitting two such modes is attained when the loop below the intersection point collapses to a cusp as seen in the inset at the bottom of Fig. 9(c) for $k_i = 1.8$. The cusp is formed as both intersection points of the loop merge together. It means that at the cusp point not only the imaginary but also the real parts of both wave numbers become equal. This point corresponds to the absolute instability at which the length of the wave packet of the global mode formed by two waves with merging wave numbers tends to infinity. Further we focus on this absolute instability which, in contrast to the convective one considered above, can be self-sustained in a sufficiently extended system. Note that the approach outlined above to find the absolute instability is an extension of the well-known cusp map for the complex frequency plane to the $(Re-\omega)$ plane [29, 30] by using the neutral stability condition $\lambda_r(Re) = 0$ which maps the real part of the growth rate λ_r to the marginal Reynolds number.

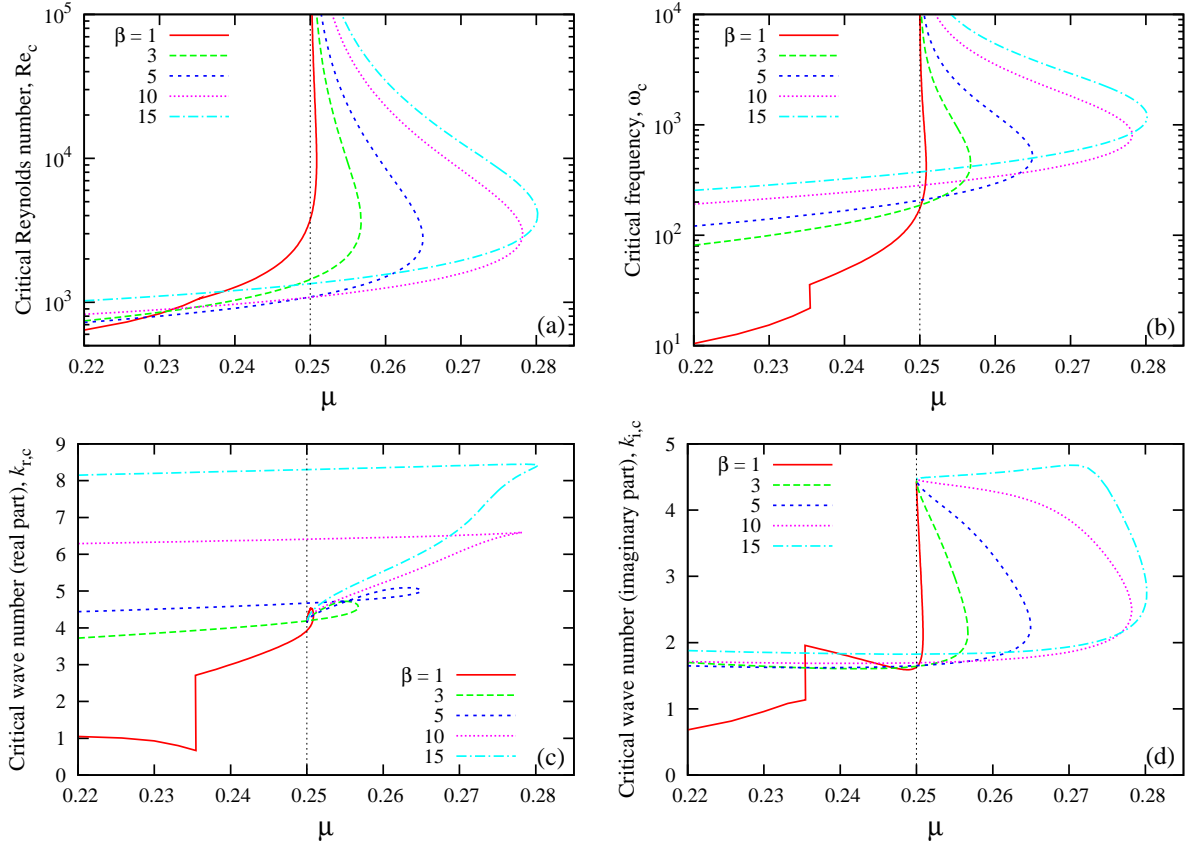


Figure 10: (a) Critical Reynolds number Re_c , (b) frequency ω_c , (c) real and (d) imaginary parts of wave number $k_{r,c}$ and $k_{i,c}$ versus μ at $Ha = 15$ and various magnetic field helicities for insulating cylinders.

The critical Reynolds number, frequency, and the critical complex wave number for the absolute instability threshold is plotted in Fig. 10 versus μ at $Ha = 15$ and various helicities of the magnetic field. Comparison with the corresponding convective instability, the critical parameters of which are plotted in Fig. 2, shows that before the Rayleigh line the threshold of absolute instability is only slightly above the convective one. The difference between both thresholds becomes significant at the Rayleigh line. Although the absolute instability extends beyond the Rayleigh line when the magnetic field is helical, the range of extension is noticeably shorter than that of the convective instability (see Fig. 13). Moreover, the upper critical Reynolds number for the absolute instability is considerably lower than that of the convective one. Although the difference between the critical Reynolds numbers for the absolute and convective instabilities is insignificant before the Rayleigh line, the critical wave numbers for the absolute instability shown in Fig. 10(c) are considerably larger than those for the convective instability [see Fig. 2b]. This difference increases with β that results in the rise of the critical wave number for absolute instability while the increase in the corresponding quantity for the convective instability threshold is insignificant. In contrast to this, the imaginary

part of the critical wave number for the lower instability branch $k_i \approx 1.8$ is almost invariable with both β and μ except for $\beta = 1$, where a jump of the instability to a larger wave number takes place at $\mu \approx 0.235$. Note that positive k_i corresponds to the amplitude of the critical perturbation growing axially downward which is an additional feature predicted by the absolute instability. Beyond the Rayleigh line the absolute instability similarly to the convective one is effective only in a limited range of Reynolds numbers which is bounded from above by the upper critical branch tending to the Rayleigh line from the right as the Reynolds number increases. The critical complex wave number is seen in Figs. 10(c) and 10(d) to tend to a certain limiting value independent of β .

2. Perfectly conducting cylinders

The neutral stability curves for perfectly conducting cylinders plotted in Fig. 11 are seen to start forming closed loops when $k_i > 0$ becoming similar to the corresponding curves for insulating cylinders shown in Fig. 9. In a certain range of k_i the curves of the critical Reynolds number plotted against the frequency in Fig.

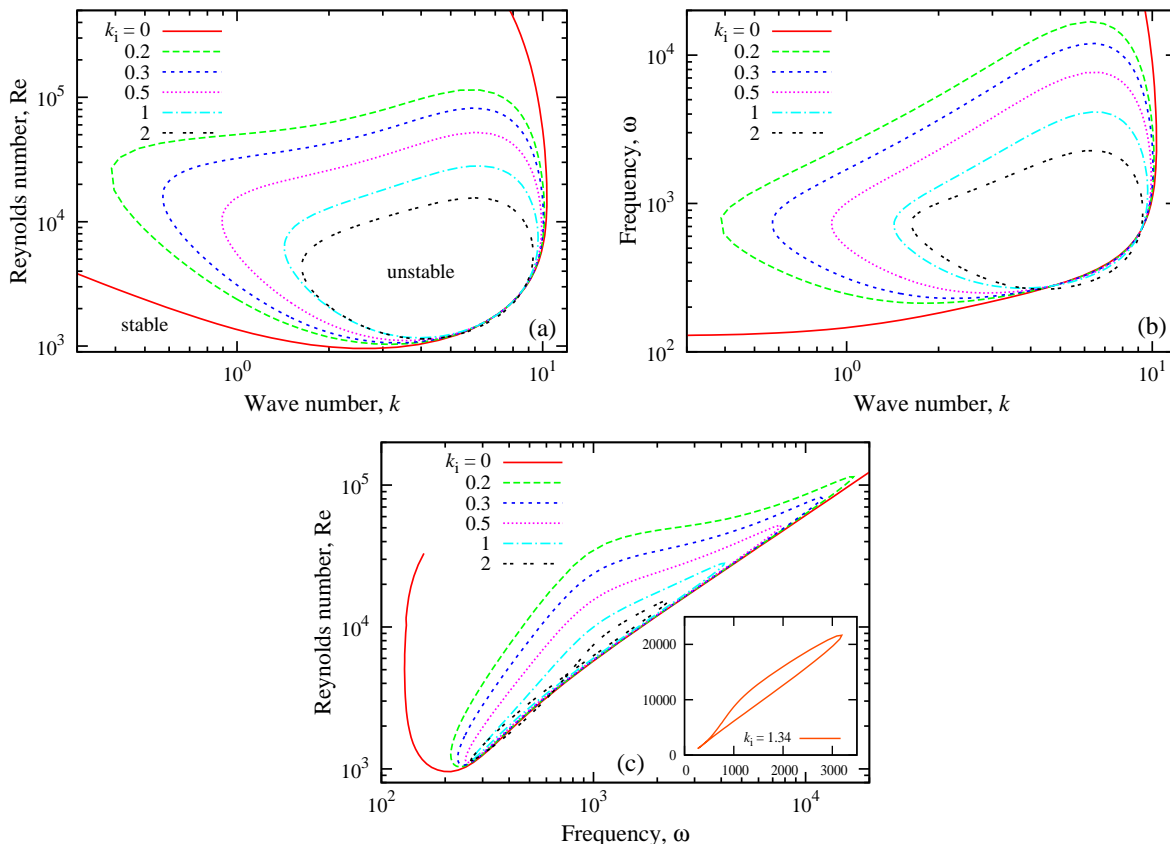


Figure 11: Neutral stability curves: (a) marginal Reynolds number, (b) the frequency versus the wave number, and (c) the Reynolds number versus the frequency for $\mu = 0.26$, $\beta = 5$ and $\text{Ha} = 15$ at various imaginary parts of wave number k_i for perfectly conducting cylinders.

11(c) intersect themselves that implies the existence of two neutrally stable modes with the same Reynolds number, frequency, and imaginary part of the wave number but different real parts of the wave number. As discussed above, two such modes can be coupled by reflections from the end walls and thus form a neutrally stable small-amplitude global mode in the system of a large but finite axial extension provided that those modes propagate in opposite directions that is implied by the variation of the marginal Reynolds number upon a small variation of k_i .

For perfectly conducting cylinders, the critical Reynolds number, frequency, and complex wave number for the absolute instability threshold plotted in Fig. 12 versus μ for $\text{Ha} = 15$ and various helicities differ significantly from the corresponding critical parameters for the convective instability threshold (see Fig. 7). First, the range of extension of the absolute instability beyond the Rayleigh line is much shorter than that of the convective instability. Note that in contrast to the convective instability there is no significant difference with respect to the extension of the absolute instability beyond the Rayleigh line between insulating and perfectly conducting cylinders (see Fig. 13). Second, beyond the Rayleigh line, similarly to insulating cylinders, for all β the range

of unstable Reynolds numbers is bounded from above by the upper critical branches which approach the Rayleigh line from the right as the upper critical Reynolds number tends to infinity. Similarly to the insulating cylinders, the corresponding critical complex wave number tends to a certain asymptotic value independent of β [see Figs. 12c and 12d]. Third, beyond the Rayleigh line the critical wave numbers for the absolute instability are noticeably greater than those for the convective instability, especially for $\beta \lesssim 10$ when the critical wave numbers for the convective instability tend to zero [see Fig. 7b].

IV. CONCLUSION

In this study we have analyzed numerically the MRI of Taylor-Couette flow with a helical external magnetic field. The problem was considered in the inductionless approximation defined by a zero magnetic Prandtl number ($\text{Pm} = 0$). First, we carried out a conventional linear stability analysis for perturbations in the form of Fourier modes specified by real wave numbers. The helical magnetic field was found to extend the original instability to a relatively narrow range beyond its purely hydrody-

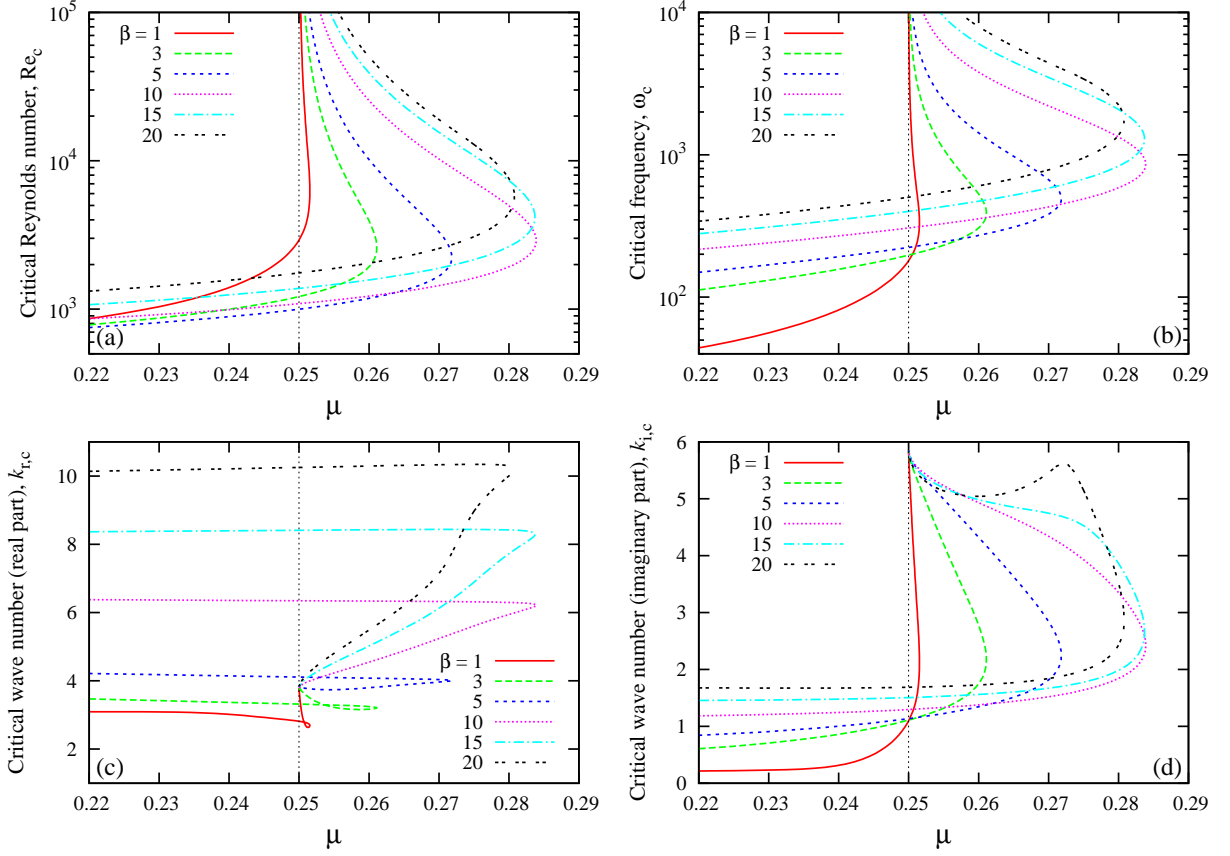


Figure 12: (a) Critical Reynolds number Re_c , (b) frequency ω_c , (c) real and (d) imaginary parts of wave number $k_{r,c}$ and $k_{i,c}$ versus μ for $Ha = 15$ and various magnetic field helicities β for perfectly conducting cylinders.

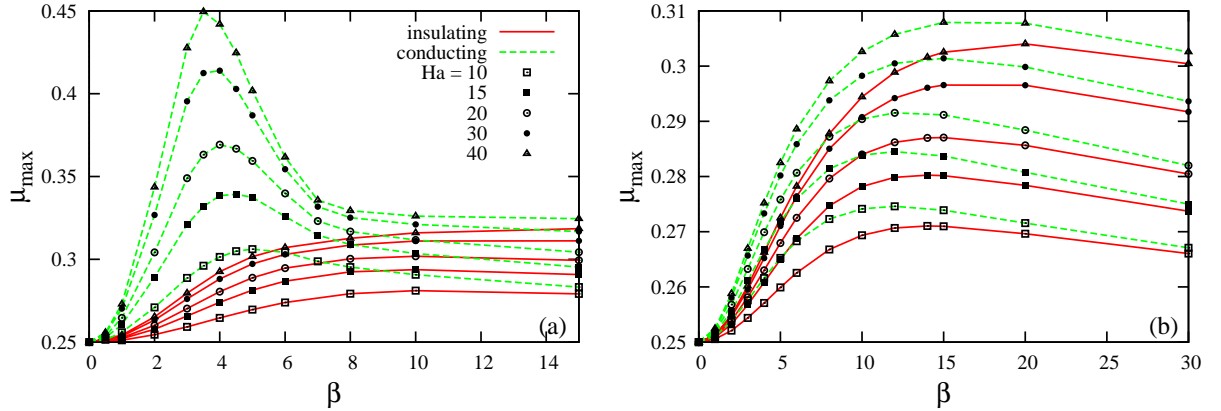


Figure 13: Maximal value of μ versus the magnetic field helicity β for (a) convective and (b) absolute instability thresholds at various Hartmann numbers for both insulating and perfectly conducting cylinders with $\lambda = 2$.

dynamic limit defined by the Rayleigh line. The range of destabilization was found to be considerably larger for perfectly conducting cylinders than that for insulating ones. For insulating cylinders, the instability beyond the Rayleigh line is effective only in a limited range of wave and Reynolds numbers. Unstable Reynolds numbers are bounded by an upper critical value which tends to in-

finitely right beyond the Rayleigh line. For perfectly conducting cylinders and moderate helicities of the magnetic field, the range of unstable wave numbers is bounded only from the short-wave end. Although there is an upper marginal Reynolds number for each unstable wave number, no bounded upper critical Reynolds number exists in this case because the range of unstable wave numbers

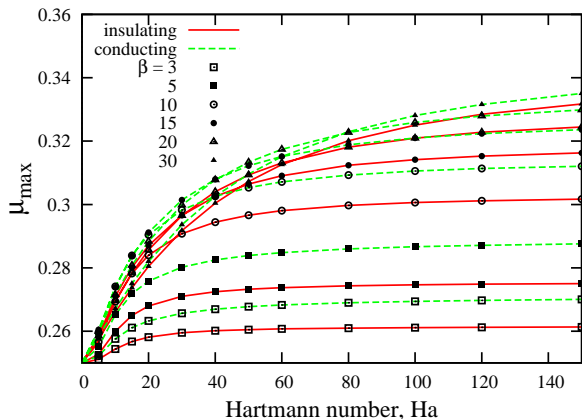


Figure 14: Maximal value of μ versus the Hartmann number for absolute instability at various β .

extends to zero, *i.e.*, infinitely long waves. Nevertheless, at sufficiently large helicities, the range of unstable wave numbers becomes bounded also from below, and an upper critical Reynolds number appears in the same way as for insulating cylinders.

It is important to note that these instabilities predicted by the conventional stability analysis in the form of single traveling waves correspond to the so-called convective instability threshold at which the system becomes able to amplify certain externally imposed perturbations that, however, are not self-sustained and thus may be experimentally unobservable without a proper external excitation. The problem is that convectively unstable perturbations grow asymptotically in time only in the frame of reference traveling with their group velocity, whereas they decay in any other frame of reference including the laboratory one. For an instability to be self-sustained and thus observable it has to grow in the laboratory frame of reference. In an extended system, this condition is satisfied by the so-called absolute instability which ensures a zero group velocity of a growing perturbation. This additional condition is satisfied by regarding the wave number as a complex quantity with a nonzero imaginary part which describes an exponential axial modulation of the wave amplitude. Using this concept, we found that there is not only a convective but also an absolute HMRI implying that this instability can be experimentally observable in a system of sufficiently large but finite axial extension. In the hydrodynamically unstable range before the Rayleigh line, the threshold of absolute instability is slightly higher than the convective one. Nevertheless, the critical wavelength for absolute instability is significantly shorter than that for the convective one that may allow us to distinguish between both. The absolute instability threshold rises significantly above the convective one beyond the Rayleigh line. As a result, the extension of the absolute instability beyond the Rayleigh line is considerably shorter than that of the convective instability without a marked difference between insulat-

ing and perfectly conducting cylinders in contrast to the convective HMRI.

The extension of HMRI beyond the Rayleigh line is of particular interest from the astrophysical point of view regarding a Keplerian velocity profile [12, 31]. For a Couette-Taylor flow with a radius ratio $\lambda = 2$ considered here, the Keplerian velocity profile approximately corresponds to a ratio of rotation rates of $\mu = \lambda^{-3/2} \approx 0.35$. As seen in Figs. 13(b) and 14 for the absolute instability, no such value of μ is reached up to $\beta = 30$ and $\text{Ha} = 150$. Whether or not it can be reached at higher β and Ha is still an open question requiring a more detailed study using either higher numerical resolution or asymptotic analysis. On the other hand, HMRI in a system of large axial extension with a radius ratio of $\lambda = 2$ might be of limited astrophysical relevance for accretion disks anyway.

Conversely to Liu *et al.* [12, 13] we find that the HMRI can be a self-sustained instability rather than just a transient growth. This contradiction may be due to a couple of additional simplifications underlying the analysis of Liu *et al.* First, the viscosity is neglected. Second, the electromagnetic force is treated as a small perturbation which is a sensible approach within the inviscid approximation where an infinitesimal magnetic field can cause a correspondingly slow growth of an unstable Fourier mode. However, such a perturbative approach may be inadequate for the absolute instability which requires a finite temporal growth rate of the corresponding convectively unstable Fourier mode. In addition, note that our results do not support the recent findings of Liu [32]. According to his estimates for the cases considered here, the absolute HMRI occurs above $\text{Re} \sim 10^5$ only. We predict the absolute HMRI to occur at the lower value of $\text{Re} \sim 10^3$, and to disappear again above $\text{Re} \sim 10^5$ due to the mechanism discussed in Sec. III A 1. This disagreement may be due to the absolute instability analysis which is carried out by Liu using real wave numbers only. According to the conventional absolute instability analysis [26, 29], such an approach yields the long-time asymptotics only in the frame of reference traveling with the group velocity of the fastest growing perturbation. Moreover, owing to its linearity, the analysis is limited to sufficiently small perturbation amplitudes only. Namely, it is limited up to the point where the first exponentially growing perturbation appears, which is the convective instability threshold.

Finally, let us compare the convective and absolute instability thresholds calculated for perfectly conducting cylinders with the experimental data of Stefani *et al.* [11] who reports on the observation of HMRI-like traveling waves at $\mu = 0.27$, $\text{Re} = 1775$, and a fixed rod current 6 kA for the coil currents $40 - 100 \text{ A}$ that corresponds to $\beta \approx 7.4 - 3$ and $\text{Ha} \approx 6.3 - 15.8$. Another observation was done at the same μ but different other parameters: $\text{Re} = 1479$, $\beta = 6$, and $\text{Ha} = 9.5$. As seen in Fig. 15, in both cases the experimental points lie well inside the range of μ for convective instability but outside that for

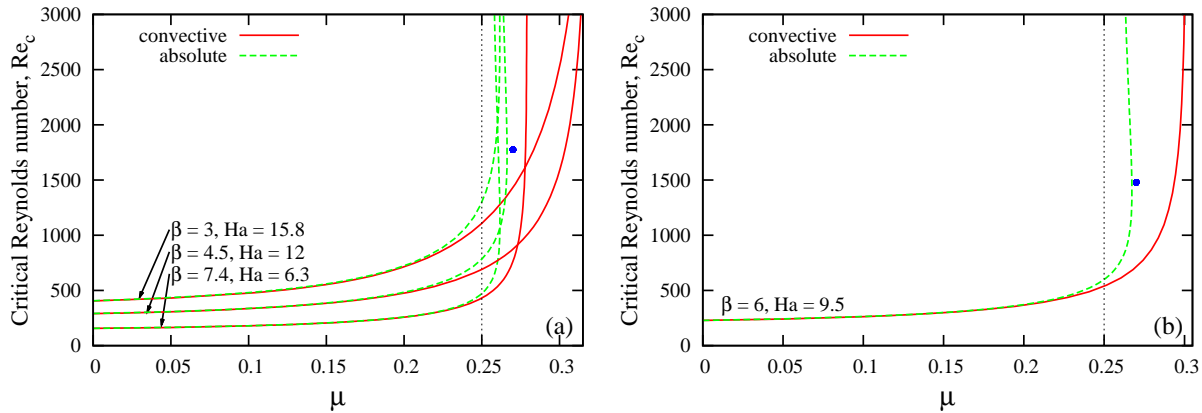


Figure 15: Comparison of the critical Reynolds number Re_c for convective and absolute instability thresholds in the case of perfectly conducting cylinders with the experimental values (dots) for which traveling waves have been observed at (a) $\mu = 0.27$, $Re = 1775$, $\beta \approx 7.4 - 3$, and $Ha \approx 6.3 - 15.8$ and (b) $Re = 1479$, $\beta = 6$, and $Ha = 9.5$.

absolute instability. This discrepancy with the experimental observations may be due to the deviation of the real base flow from the idealized one used in this study. In particular, the Ekman pumping driven by the end walls in the experiment, which is not taken into account in the present analysis, may affect the hydrodynamic stability limit of the base flow, *i.e.*, its actual Rayleigh line, which however serves as the reference point for the observation of MRI. A more detailed comparison with the experimental observations lies outside the scope of the present paper.

In conclusion, the main result of the present paper is the finding of absolute HMRI in addition to the convective one which can be self-sustained and, thus, ex-

perimentally observable without external excitation in a system of sufficiently large axial extension. A characteristic feature of HMRI is the upper critical threshold existing besides the lower one that distinguishes it from a magnetically-modified Taylor vortex flow.

Acknowledgments

This research was supported by Deutsche Forschungsgemeinschaft in frame of the Collaborative Research Centre SFB 609. We would like to thank Frank Stefani and Thomas Gundrum for stimulating discussions.

-
- [1] E. P. Velikhov, Sov. Phys. JETP **36**, 995 (1959).
 - [2] S. Chandrasekhar, Proc. Natl. Acad. Sci. U.S.A. **46**, 253 (1960); *Hydrodynamic and Hydromagnetic Stability* (Oxford University Press, London, 1961).
 - [3] S. A. Balbus and J. F. Hawley, Astrophys. J. **376**, 214 (1991).
 - [4] S. A. Balbus and J. F. Hawley, Rev. Mod. Phys. **70**, 1 (1998).
 - [5] D. R. Sisan, N. Mujica, W. A. Tillotson, Y.-M. Huang, W. Dorland, A. B. Hassam, T. M. Antonsen, and D. P. Lathrop, Phys. Rev. Lett. **93**, 114502 (2004).
 - [6] H. Ji, M. Burin, E. Scharfman, and J. Goodman, Nature (London) **444**, 343 (2006).
 - [7] J. Goodman and H. Ji, J. Fluid. Mech. **462**, 365 (2002).
 - [8] R. Hollerbach and G. Rüdiger, Phys. Rev. Lett. **95**, 124501 (2005).
 - [9] G. Rüdiger, R. Hollerbach, F. Stefani, Th. Gundrum, G. Gerbeth, and R. Rosner, Astrophys. J. **649**, L145 (2006).
 - [10] F. Stefani, Th. Gundrum, G. Gerbeth, G. Rüdiger, M. Schultz, J. Szklarski, and R. Hollerbach, Phys. Rev. Lett **97**, 184502 (2006).
 - [11] F. Stefani, Th. Gundrum, G. Gerbeth, G. Rüdiger, J. Szklarski, and R. Hollerbach, New J. Phys. **9**, 295 (2007).
 - [12] W. Liu, J. Goodman, I. Herron, and H. Ji, Phys. Rev. E **74**, 056302 (2006).
 - [13] W. Liu, J. Goodman, H. Ji, Phys. Rev. E **76**, 016310 (2007).
 - [14] W. Liu, Phys. Rev. E **77**, 056314 (2008).
 - [15] L. Landau and E. M. Lifshitz, *Fluid Mechanics* (Pergamon, London, 1987), Sec. 28.
 - [16] Yu. B. Ponomarenko, J. Appl. Mech. Tech. Phys. **14**, 775 (1973).
 - [17] A. Gailitis and Ya. Freibergs, Magnetohydrodynamics **12**, 127 (1976).
 - [18] A. Gailitis and Ya. Freibergs, Magnetohydrodynamics **16**, 116 (1980).
 - [19] P. Huerre and P. A. Monkewitz, Annu. Rev. Fluid Mech. **22**, 473 (1990).
 - [20] S. M. Tobias, M. R. E. Proctor, and E. Knobloch, Physica D **113**, 43 (1998).
 - [21] M. R. E. Proctor, S. M. Tobias, and E. Knobloch, Physica D **145**, 191 (2000).
 - [22] J. Priede, I. Grants, and G. Gerbeth, Phys. Rev. E **75**, 047303 (2007).
 - [23] I. Herron and J. Goodman, Z. Angew. Math. Phys. **57**, 615 (2006).

- [24] G. Rüdiger, R. Hollerbach, M. Schultz, and D. A. Shalybkov, *Astron. Nachr.* **326**, 409 (2005).
- [25] A. G. Kulikovskii, *Prikl. Mat. Mekh.* **30**, 148 (1966) [*J. Appl. Math. Mech.* **30**, 180, (1966)].
- [26] E. M. Lifshitz and L. P. Pitaevskii, *Physical Kinetics* (Pergamon, London 1981), Secs. 62 and 65.
- [27] J. Priede and G. Gerbeth, *Phys. Rev. E* **56**, 4187 (1997).
- [28] J. R. Briggs, *Electron-Stream Interaction with Plasmas* (MIT Press, Cambridge, MA, 1964).
- [29] P. J. Schmid and D. S. Henningson, *Stability and Transition in Shear Flows*, (Springer, New York, 2001), Secs. 7.2.1–7.2.3.
- [30] K. Kupfer, A. Bers, and A. K. Ram, *Phys. Fluids* **30**, 3075 (1987).
- [31] G. Rüdiger and R. Hollerbach, *Phys. Rev. E* **76**, 068301 (2007).
- [32] W. Liu, *Astrophys. J.* **692**, 998 (2009)